Industrial Chemistry & Materials

ROYAL SOCIETY OF CHEMISTRY

PAPER

View Article Online
View Journal | View Issue

Cite this: *Ind. Chem. Mater.*, 2024, **2**, 469

Influence of surfactants on selective mechanical separation of fine active materials used in high temperature electrolyzers contributing to circular economy†

Sohyun Ahn, * Suvarna Patil and Martin Rudolph

As one of the promising hydrogen production technologies, the development of water electrolysis systems including recycling of their functional components is actively investigated. However, the focus lies on energy and chemical intensive metallurgical operations and less on mechanical separation processes in most studies. Here, an innovative surfactant-based separation process (using CTAB and SDS) is investigated to contribute to developing a selective physical separation process for ultrafine particles used in high temperature water electrolyzers (composed of NiO, LSM, ZrO_2, and YSZ). Their different surface charge in alkaline solutions influences the adsorption of surfactants on particle surfaces as well as the modification of particulate wettability, which is a key separation feature. Through the observations of changes in surface charge and wetting behavior in the presence of surfactants, a feasibility of liquid–liquid particle separation (LLPS) is evaluated. The performance of LLPS with model particle mixtures shows the potential of selective separation with recovery of NiO in the organic phase, while the rest of the particles remain in the aqueous phase. Perovskite LSM is not considered in this system because it shows a high possibility of being recovered by magnetic separation. The proposed process can be further optimized by increasing the phase separation stages, and further research is needed on the NiO phase, which showed exceptional behavior in the presence of the surfactants.

Received 26th April 2024,
Accepted 5th July 2024

DOI: 10.1039/d4im00044g

rsc.li/icm

Keywords: Fine particle separation; Solid oxide electrolyzer; Recycling; Particle surface modification.

1 Introduction

The utilization of hydrogen as an alternative energy source is becoming increasingly crucial in order to facilitate the transition from fossil-based to renewable sources and to achieve carbon neutrality by 2050.[1,2] Green hydrogen based on electrolysis and renewable energy is the cleanest hydrogen with no carbon emissions in the production processes, but due to yet high prices it occupies a tiny percentage of the overall global hydrogen market.[3,4] Consequently, water electrolysis technology is being developed and scaled up globally.[5]

Four major types of water electrolyzers have been developed including high temperature electrolyzers (HTELs) and performance development studies have been carried out for all four types.[4–7] The other three types are polymer electrolyte membrane electrolyzers (PEMs), anion exchange membrane electrolyzers (AEMs), and alkaline water electrolyzers (AWEs). In contrast to HTELs, the other three electrolysis systems operate at low temperatures (below 200 °C). The aim of this study lies into investigating the recycling aspect of HTELs, which are also commonly referred to as solid oxide electrolysis cells (SOECs). The operating temperature is between 800 °C and 1000 °C under high-pressure conditions. High temperature increases the efficiency of the cells up to 90% and in this respect, non-noble catalysts based on critical raw materials like nickel and rare earth elements (REEs) are required.[8] However, the degradation of the electrolyte is inevitable due to the extreme conditions. Currently the reported lifetime of HTELs is 20 000 h, which is shorter than those of other electrolyzer types (PEM: 50 000 h, AEM: 30 000 h, AWE: 60 000).[9–11] Since the lifetime of electrolyzers is limited, studies on long-term operation, development of alternative materials, and research in recycling have attracted attention. An understanding of the structure and materials used in

Helmholtz-Zentrum Dresden-Rossendorf, Helmholtz Institute Freiberg for Resource Technology, Chemnitzer Straße 40, Freiberg 09599, Germany.
E-mail: s.ahn@hzdr.de

† Electronic supplementary information (ESI) available. See DOI: https://doi.org/10.1039/d4im00044g

electrolyzers is crucial in order to develop efficient recycling processes.

The electrolysis system commonly consists of repeating units of stacks comprising membrane electrode assemblies (MEAs) and separating plates like end plates, cell frames, and interconnects. Mainly, HTEL MEAs (*i.e.* cells) are structured with the solid electrolyte layer, the hydrogen electrode (fuel side), the oxygen electrode (air side), and the barrier layer (see Fig. 1). The most typical oxygen-ion conducting electrolyte material is yttrium stabilized zirconia (YSZ, 3 to 8% (n/n) of Y_2O_3 doped on ZrO_2) for high temperature operating conditions (over 700 °C).[8,12] Other materials under consideration for the intermediate temperature range are scandium stabilized zirconia (ScSZ), ceria-based materials or lanthanum containing materials. The catalysts used for the oxygen evolution reaction (OER) are perovskite type materials such as lanthanum strontium manganite (LSM) and lanthanum strontium cobalt ferrite (LSCF).[13] As an interlayer, gadolinium-doped ceria (GDC) is applied to prevent the interaction between the electrolytes and air-electrode materials. The nickel-based cermet is used on the fuel-side electrode for the hydrogen evolution reaction (HER).[14,15] However, alternative materials are currently being investigated due to the depletion of active materials such as nickel after long-term operation.[16]

Intending to scale up the hydrogen electrolyzer capacity, recycling strategies are becoming increasingly important as the amount of (critical) materials needed for the system increases. A study by Férriz *et al.* classified the common materials used in the electrolyzers by cost value, criticality, and environmental hazardousness and emphasized on the importance of recycling strategies.[17] The dominant materials used in the MEAs such as nickel, rare earth elements (*e.g.* La, Ce, Gd, and Y) or cobalt are on the list of critical raw materials in the EU.[18] A number of studies have highlighted the lack of literature on the recycling of solid oxide cells (SOCs) and have proposed potential recycling strategies based on state-of-the-art materials. However, a significant proportion of the reported methodologies are constrained to hydrometallurgical treatments.[19–21] Chemical processes are typically considered to be responsible for recovery of critical raw materials, still they consume high energy and discharge more wastewater as well as waste gas compared to physical recycling processes. Conversely, mechanical process approaches offer the advantages of low energy consumption and environmentally friendly short recovery routes. Many studies have presented a probability of mechanical processes for the recovery of valuable components from spent LIBs and fine fractions from the black mass.[22,23] Consequently, an investigation of the mechanical processes for recycling the critical raw materials used in electrolyzer cells should be also considered. In particular, ultra-fine particles (below 10 μm) containing active materials are generated following the previous separation processes such as de-coating, disassembly, and milling processes, and also essential to be recovered.[24,25]

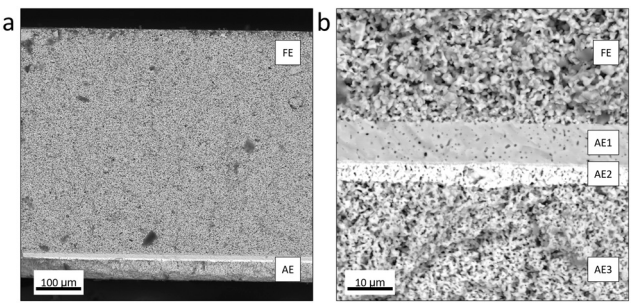

Fig. 1 Cross sectional back scattered electron scanning electron microscopy (BSE-SEM) images of the HTEL MEA. (a) Magnification of 400; (b) magnification of 4000. FE: fuel side electrode including its substrate layer, AE1: solid electrolyte, AE2: barrier, AE3: air side electrode.

Given the above, we investigate potential mechanical separation processes, with a particular focus on wet chemical methods for ultra-fine particles in HTELs. To develop effective separation processes, physicochemical surface properties of the pristine materials are characterized. Since the materials have similar chemical and physical properties, it is challenging to recover them selectively. Therefore, the introduction of modifying reagents helps to enhance the selective recovery of the targeted particles, with surfactants in particular modifying the surface properties.[26,27] The molecular characteristics of surfactants such as alkyl chain length, molecular size, and functional groups influence both the reduction of interfacial tension and their adsorption ability. Surfactants are divided into four categories by the head groups: non-ionic, cationic, anionic and amphoteric. Based on the particle surface charge, respective surfactants adsorb on the surface through electrostatic interactions resulting in a change of wettability. Therefore, a study on surfactant-based methods provides a potential way for the selective separation of HTEL particles. The surfactants considered in this paper are sodium dodecyl sulfate (SDS) and cetyltrimethylammonium bromide (CTAB). SDS is one of the most extensively studied anionic surfactants and is used in mineral processing to recover hydrophilic particles by selectively adsorbing on the particulate surface.[28,29] The cationic surfactant, CTAB, is widely used and can hydrophobize negatively charged particles and is also quite active in the liquid–gas interface.[30,31] The influence of the two respective surfactants on the particle surface properties and their wetting behaviour are studied. Here, a new method, liquid–liquid particle phase transfer is introduced to investigate the wettability of sub-micron particles as well as to separate them. A conventional liquid–liquid extraction is one of the well-known methods to separate target compounds, which are usually liquids or dissolved components, exploiting the difference in solubility of two immiscible phases.[32,33] In mineral processing, this method has been developed further to recover ultrafine particles, which are only inefficiently recovered by conventional flotation.[34] Parameters such as solution pH, the

concentration of reagents, the interfacial tension of oil and water, *etc.* play an important role.[35–38] However, to the best of our knowledge, this method has not been studied in the field of recycling HTEL cells. In our previous work, selective separation of ultrafine active materials was accomplished with over 97% of recovery through surfactant based liquid–liquid particle separation (LLPS) of ultrafine particles in PEM water electrolyzer recycling.[39] Ultimately, this method is applied to separate the HTEL model particle mixture in this study.

2 Results and discussion

2.1 Influence of surfactants

2.1.1 Interfacial tension. The surface tension of water is 72 mN m^{-1} due to the strong cohesion forces between water molecules and that of cyclohexane is 25 mN m^{-1} at 20 °C.[40,41] Upon addition of surfactants in the liquid–liquid system, the polar ends of the surfactant are oriented to the polar phase (water) and the alkyl chain to the non-polar phase (cyclohexane) so that the presence of the surfactant reduces the interfacial tension. Table 1 presents the interfacial tensions between water and cyclohexane at different concentrations of CTAB and SDS.

The interfacial tension between water and cyclohexane is approximately 46.4 mN m^{-1}, which is consistent with a former study with 48.9 mN m^{-1}.[41] At higher concentrations of CTAB this value decreases to 6.8 mN m^{-1}. At concentrations above 5×10^{-4} M, the cyclohexane droplets could no longer remain adhered to the tip and directly disappeared after expelling the drop, resulting in no possible measurement. However, with the same concentrations of SDS, the interfacial tension decreases much less. The critical micelle concentration (CMC) of SDS is reported to be 8.0–8.2 mM, while that of CTAB is reported to be 0.9–1 mM.[42] These concentrations are above the considered concentrations in this study. However, this emphasizes the strong presence of surfactants in the liquid–liquid interface which may affect the effective particle mitigation through the interface during micro-particle separation.

2.1.2 Zeta potential in the presence of the surfactant. The solid electrolyte materials are negatively charged at pH 10 with initial zeta potentials of −25 mV and −28 mV whereas electrode materials show positive zeta potentials of +12 mV and +30 mV, respectively (see Fig. 2). The surfactant adsorption depends on the particle surface charge and the functional chemical group of the surfactant. When the amphiphiles are added to the suspension of oppositely charged particles, the ionic terminal group is attracted to the particle surface. Once the surfactant is fully adsorbed forming a single layer on the particle surface, most likely in the form of hemimicelles, the charge is compensated and an isoelectric point is reached. With an excessive amount of surfactant, hydrophobic interactions between the alkyl tail part of the molecules contribute to the conversion of the electric charge to the opposite due to bilayer formation.[27] Consequently, identifying the concentration of the surfactant that causes such an iso-electric point is vital to render the particle surface hydrophobic.

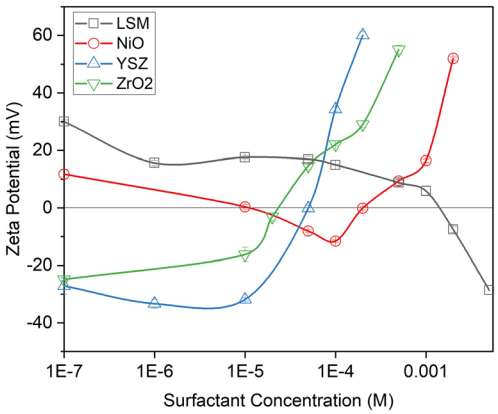

Fig. 2 Zeta potential of representative materials in the presence of oppositely charged surfactants: SDS (for LSM and NiO) and CTAB (for YSZ and ZrO_2) at pH 10. The lines are guides for the eye and error bars indicate 95% of confidence interval.

An isoelectric point for YSZ is shown at a CTAB concentration of 2×10^{-5} M, while it was at 5×10^{-5} M for ZrO_2. The obtained values are close to the result of the calculation based on their specific surface area and head-group area for each surfactant. (Table S1 in the ESI†). Further increasing the concentration of surfactant causes the adsorption of the surfactant bilayer and increases the repulsive electrostatic force between the particles.

Concerning the electrode material, the surface charge of LSM converted to negative in the presence of 2×10^{-3} M SDS. The zeta potential of NiO exhibits a different behaviour, with an initial decline observed until 1×10^{-4} M of SDS, followed by an unexpected increase and even reversal to positive values. We lack studies with respect to the surface charge of NiO, particularly upon adsorption of surfactants. Indeed, further adsorption of SDS in bilayer formation would result in a more negative surface charge, so the positive zeta potentials must somehow come about due to disassociation of NiO and adsorption of ionic Ni^{2+} species. The measurement is repeated several times and the behavior is quite reproducible. Further investigation on this interesting phenomenon is required, in addition to the identification of other unexpected behaviour of NiO exhibited below.

Table 1 Interfacial tension between water and cyclohexane with different concentrations of CTAB and SDS at room temperature, errors account for the 95% confidence interval

Concentration (M)	Interfacial tension (mN m^{-1})	
	CTAB	SDS
0	46.4 ± 0.2	
1×10^{-6}	29.9 ± 0.3	45.1 ± 0.1
1×10^{-5}	19.6 ± 0.1	42.2 ± 0.1
1×10^{-4}	6.8 ± 0.0	34.8 ± 0.3
5×10^{-4}	—	26.8 ± 0.1
1×10^{-3}	—	23.5 ± 0.1

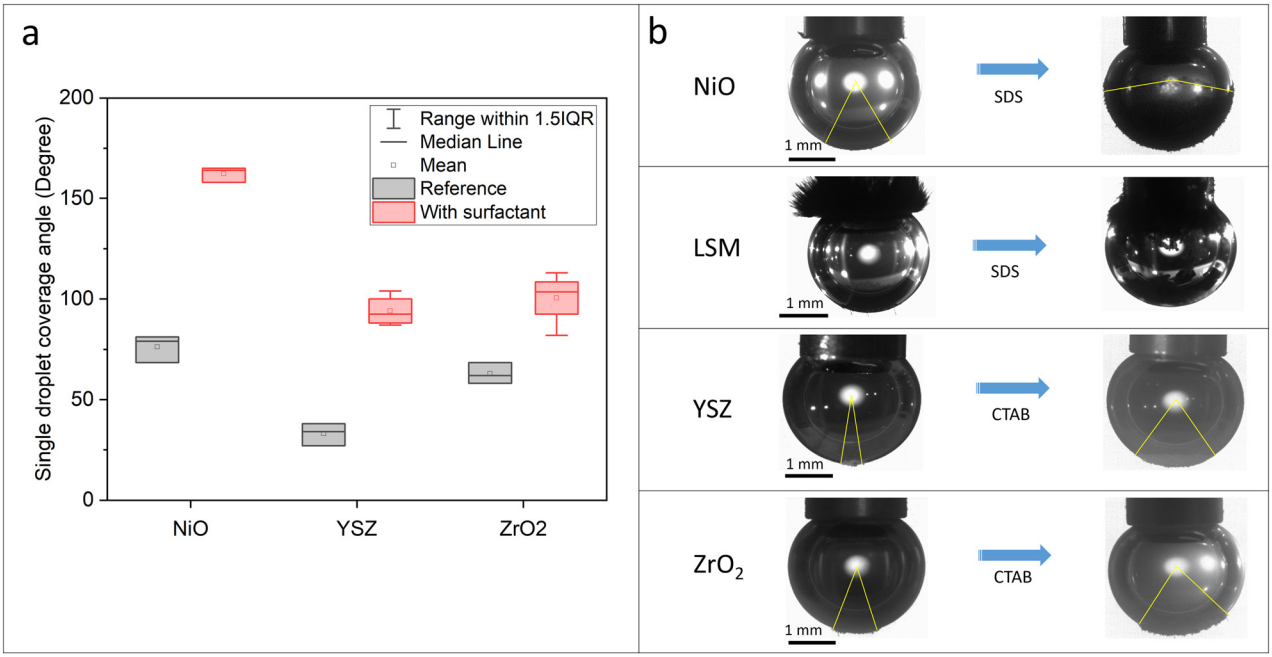

Fig. 3 Images of particles attached on the cyclohexane droplet at pH 10. (a) Box plot of the measured coverage angle. Black boxes present inherent attachment of the particles on the cyclohexane droplet. Red boxes indicate the degree of the coverage angle in the presence of the respective surfactant; (b) first images show the reference result of each particle wettability (without surfactant) and second images represent the change of wetting behavior of the particles after adding the surfactant at the concentration where charge compensation occurred, *i.e.* statistically monolayer coverage is achieved.

2.1.3 Single droplet attachment. In Fig. 3, the changes of particle surface wettability in the presence of corresponding surfactants are shown with a box plot representation. The amount of attached particles on the cyclohexane droplet surface increased by adding the corresponding surfactant. The droplet coverage angle of NiO is increased from 75° to 170° by adding the surfactant concentration where charge compensation occurred, *i.e.* statistical monolayer coverage. Without surfactant, only a few particles of YSZ and ZrO_2 are attached to the cyclohexane droplet surface with a slight coverage angle of 32° and 64°, respectively. After conditioning with CTAB, more particles are attached on the cyclohexane surface, showing the coverage angle of 100° for both types of materials.

Unlike other particles, the coverage angle of LSM could not be quantified. After mixing the suspension, the particles attached to the end of the steel capillary most likely due to magnetic interactions. The morphology of the attached particle assembly appears like aligning with a magnetic field. Following the addition of the corresponding surfactant, observations of hydrophobized particle behavior are detected but quantification remains impossible. It is however quite remarkable to showcase the competing magnetic and hydrophobic interactions in this case. Fundamentally, the presence of sufficient manganese lattice ions may result in magnetic properties by double exchange mechanisms.[43] The magnetic properties of LSM ($La_{1-x}Sr_xMnO_3$, with x as a doping level) are influenced strongly by the x value and the material used in this study has an x-value of 0.2, which was confirmed as a superparamagnetic material with S-shaped magnetic hysteresis loops in a study by Turky *et al.*[44,45] Accordingly, the liquid–liquid separation model particle mixture may exclude LSM, depending on the degree of the impact of the surfactant on LSM hydrophobicity. As previously outlined by Boelens *et al.*, high-gradient magnetic separation may be employed to facilitate the separation of LSM from particle mixtures.[46]

2.1.4 Liquid–liquid particle separation (LLPS) – single system. The investigation of single particle behaviour in LLPS allows the surfactant adsorption on the particle surface to be identified, as well as the possibility of a selective separation process. To ascertain the selective adsorption of target surfactants on the particle, demonstrations for both types of surfactants are compared. The electrostatic repulsive force between similarly charged particles and the surfactant is expected to prevent adsorption, thereby serving as a reference to highlight the selective adsorption behavior.[47]

Fig. 4 depicts the recovered amount (in % (w/w)) of the particles in the aqueous phase, which represents the degree of hydrophilic behavior. Since all pristine particle fractions have a strong affinity for water (by means of contact angles), large amounts of particles are expected to be recovered in the aqueous phase. Theoretically, solid electrolyte materials should be hydrophobized by electrostatic attractive force only with CTAB whereas the anionic surfactant SDS adsorbs exclusively on the electrode functional particles at pH 10.

However, NiO demonstrated an unexpected transfer behaviour, whereby even in the absence of a surfactant, 85%

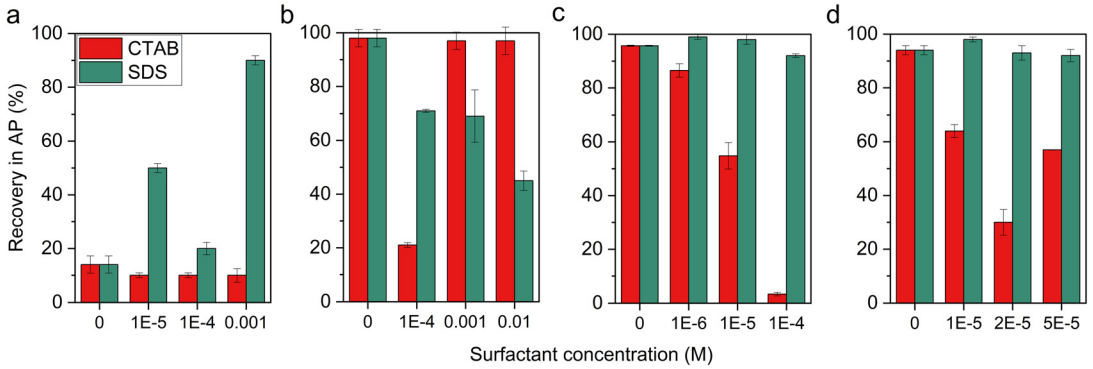

Fig. 4 Phase separation of the single particle system: (a) NiO; (b) LSM; (c) YSZ; (d) ZrO_2. The recovered particles in the aqueous phase (AP) subsequent to the surfactant concentration at pH 10 in % (w/w), error bars indicate 95% of confidence interval.

(w/w) of the particles are recovered in the organic phase, rather than in the aqueous phase. When individual surfactants are added to the particle suspension, no clear tendency is demonstrated for the effect of the target surfactant on the particle surface. Presuming that the particle surface is hydrophobic, hydrophobic interactions are recognized as a driving force for the surfactant adsorption.[48] The tails of the SDS will be adsorbed on the surface and the heads will be directed to the outer layer. If it is assumed that this effect would result in more particles recovered in the aqueous phase, the same result would be expected when CTAB is added. However, CTAB does not show to affect the wettability of the particles, which could be due to repulsion of the positively charged CTAB from the NiO surface avoiding such hydrophobic adsorption. So while it is recognized that there is electrostatic adsorption between NiO and the surfactants, it is difficult to define the exact mechanism.

Partial transfer occurs in the presence of target surfactant SDS in the LSM suspension. At the highest concentration (0.01 M), nearly 50% of the particles are transferred to cyclohexane. Nevertheless, the addition of the surfactant above the CMC provokes the formation of stable emulsions and suppresses the effective separation processes. The unexpected transfer of LSM to the organic phase at a low CTAB concentration of 1×10^{-4} M, as opposed to the expected repulsion between similarly charged systems, will require further investigation. At higher CTAB concentrations, LSM sustained its rather hydrophilic nature as expected.

In the alkaline solution, approximately 95% of the solid electrolyte particles are recovered in the aqueous phase. The addition of the cationic surfactant results in an increase in the number of transferred particles to the organic phase. With increasing surfactant concentration in the YSZ suspension, the surfactant changes the wetting properties and enables up to 97% of particles to be recovered with the cyclohexane phase. In the case of ZrO_2, 2×10^{-5} M of CTAB contributes to 70% transfer. When a higher amount of CTAB is added, the surfactant bilayer is formed so that more particles are recovered in the aqueous phase again. Surface modification by the addition of the anionic surfactant is insignificant for both ZrO_2 and YSZ, as they remain highly affine to the aqueous phase.

2.2 Separation processes

2.2.1 Investigation of NiO wetting behavior. As previously described in the context of single particle LLPS, the transfer of NiO fractions to the organic phase at pH 10 in the absence of surfactants was observed to be greater than 80%, despite the low water contact angle of 32° (*cf.* Table 2). Common metal oxides including NiO are hydrophilic in nature due to many polar sites on their surfaces.[49] A possible hypothesis of its high affinity with organic solvent is that the outer layer of nickel particles becomes hydroxylated when they are immersed in water at high pH. OH-groups terminate their surface and evolve to $Ni(OH)_2$ under alkaline conditions and this is confirmed by a few studies.[50–52] A study by Micale *et al.* explained that the polar site concentration of particle surfaces is related to the crystallographic characteristics, particularly a ratio of the edge area to basal area of the particle. According to their study, the surface of $Ni(OH)_2$ became partially hydrophobic with a higher ratio of the basal face plane to crystal edge, which was consistent with a study

Table 2 Physical properties of the representative materials used in HTELs, errors account for the 95% confidence interval

	NiO	LSM	ZrO_2	YSZ
Applications	Air side electrode	Fuel side electrode	Electrolyte	Electrolyte
$d_{50.3}$ (μm)	1.1 ± 0.1	1.0 ±0.1	2.2 ± 0.2	0.9 ± 0.1
Water contact angle (degree)	32 ± 2	36 ± 4	32 ± 1	34 ± 3
Iso-electric point, IEP	N/A	N/A	pH 8.2	pH 8
BET surface area (m^2 g^{-1})	80.3 ± 1.8	5.3 ± 0.1	23.5 ± 0.2	7.9 ± 0.1

from Chang *et al.*, which also revealed that the hydrophobicity changes depending on the degree of disorder.[53,54] In addition, Azimi *et al.* found that metals and ceramics can also have hydrophobic surfaces, as their electronic structure may hinder hydrogen bonding with water.[55] A paper from Eslamibidgoli *et al.* supports the argument that water adsorption is related to the electronic structure and addresses that $Ni(OH)_2$ is naturally hydrophobic.[56]

To confirm its wetting behavior, particles were dispersed in two immiscible component systems at different pH values. As seen in Fig. 5, NiO particles partially transferred to the organic phase (top) even under acidic conditions due to the change of the outer layer of particles, which supports the previous studies. Unlike the well-known hypothesis that metal oxides are hydrophilic, each particle transferred to the organic phase like hydrophobic particles and forms a stable emulsion layer at pH 9 and 11 even without any addition of surfactant. According to the pH of the dispersion through this preliminary test, different particle wetting behaviors have been confirmed. Consequently, the design of the separation process needs to be changed considering the special behavior of NiO in the alkaline solution.

2.2.2 Model mixture with different types of surfactants and dispersants. Due to the hydrophobic behavior of the Ni phase in alkaline solutions, further considerations have been taken into account, as the application of reagent mixtures allows a combination of desired properties.[57] The aim of this test was to observe which cases the particles could be separated most effectively, and therefore the results are only visually observed and not quantified. The considered parameters are: dispersant, surfactant, and pH. Three types of dispersants, sodium oleate (NaOL, $C_{18}H_{33}O_2Na$), citric acid ($C_6H_8O_7$) and sodium hexametaphosphate (SHMP, $(NaPO_3)_6$) have been tested to stabilize particles expected to be found in the aqueous phase. The effectiveness of CTAB, SDS and polyethylene glycol (PEG) as a surfactant has been investigated. In Fig. 6, five examples of the combination are shown and further images can be found in the ESI† (Fig. S4 to S6). The pH of the suspension is either 8 or 11. At pH 8, hetero-coagulation of the oppositely charged particles is prevented, however at pH 11 the hydrophobic behaviour of NiO is prominently

Fig. 5 NiO particle suspensions in two immiscible liquid systems (top: cyclohexane, bottom: DI water at different pH values). From left to right, pH 3, 5, 7, 9, and 11.

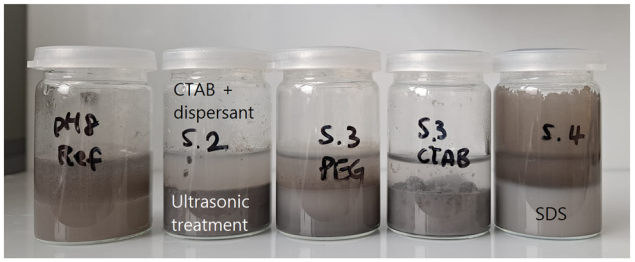

Fig. 6 Five different combinations of surfactants and dispersants in two immiscible liquid systems (top: cyclohexane, bottom: DI water, from left to right: S1–S4) S1: reference mixture at pH 8, S2: CTAB + citric acid and ultrasonic treatment included in the process, S3: PEG and CTAB as a surfactant, S4: SDS as a surfactant.

observed. Additionally, the influence on the order of adding reagents is considered for efficient separation.[58] But no significant differences have been found in the separation method between adding the surfactant first and dispersant later and *vice versa*.

The glass bottle on the left end in Fig. 6, S1 represents a reference, which contains the particle mixture without any types of reagents at pH 8. As expected, particles of NiO are partially transferred to the organic phase. The S2 is prepared with the following steps: the pH is adjusted to 4 to avoid hetero-coagulation between solid electrolyte particles and NiO, and CTAB is added later. By adjusting the pH to 11, CTAB is adsorbed on the negatively charged solid electrolyte particles. Citric acid is added to make a stable dispersion of the NiO particle in the aqueous phase. This is because in a single-particle system, CTAB has been shown to not change the hydrophobicity of the Ni phase in the alkaline solution (Fig. 4), while citric acid stabilizes them in the aqueous solutions (Fig. S4†). Interestingly, most of the particles are transferred to the organic phase despite considering the aforementioned parameters, and after the ultrasonic treatment, entrapped NiO particles moved to the aqueous phase. The pH set up for S3 is 8, aiming to recover NiO particles in water and solid electrolyte particles in cyclohexane by adding citric acid first, and then the surfactant (PEG). The second S3 bottle is prepared with the identical procedure but the surfactant (CTAB) is added after adjusting the pH to 11. However, most of the particles rather stabilized in water despite being in the presence of the surfactant. The most effective configuration is the addition of SDS at pH 8, which shows the closest in color to white in the aqueous phase representing YSZ and ZrO_2, and gray NiO particles in the organic phase. This method is chosen for the separation process studied further.

In addition, considerable amounts of particles are influenced by sonication treatment. For instance, the particles in the organic phase moves to the aqueous phase. In sonication, most importantly cavitation effects show great potential to stabilize particle dispersion by breaking down the clusters of particles.[59] The ultrasonic bath is used in this study because ultrasonic probes provide a stronger power,

which likely causes the formation of macro-emulsions, and it is not desirable for effective separation. Including an ultrasonic treatment for 10 min (Bandelin, RK 103H, Germany, ultrasonic peak power 560 W, nominal ultrasonic power 140 W, ultrasound frequency 35 kHz) during the process may lead to the phase transfer of the particles.

2.2.3 Liquid–liquid particle separation – mixture system. As aforementioned, LSM has the potential to be recovered by magnetic separation rather than by the application of surfactants in LLPS stemming from only partial recovery despite the use of a high concentration of surfactant. Hence, particle mixtures for the liquid–liquid mixed microparticle selective separation contain only NiO, YSZ and ZrO_2 in this study. Since the preference of pristine NiO particles is in the organic phase and not the aqueous phase under alkaline pH conditions, the experiment is designed to recover electrode materials in the organic phase and solid electrolyte materials in the aqueous phase. The particulate dispersion is prepared with DI water at pH 8 to avoid hetero-coagulation due to attractive double layer interactions and the corresponding concentration of SDS is added. An ultrasound bath sonication step is included after the agitation of the two-liquid dispersion.

Although the pH is adjusted to avoid hetero-coagulation between different particles, over 95% of the particles attract each other and are transferred to the organic phase. (Fig. 7) The stability of these heteroaggregates depends on the relative particle sizes. For instance, irregular unstable clusters are formed between similar sized particles but when the smaller particles (*i.e.* NiO) fully cover the surface of the larger ones (*i.e.* ZrO_2) the surface properties of the entire stable cluster is defined by the smaller particles.[60] Another hypothesis is the reduction of the electrostatic repulsion on hydrophobic surfaces causing an attractive interaction between the particles.[61] The degree of hetero-coagulation is attributed to the hydrophobicity of the particles and is higher with increasing hydrophobicity.[62] Hence, even for solid electrolyte particles which are hydrophilic, most of them form emulsions and are entrapped between cyclohexane droplets.

By increasing the surfactant concentration, de-agglomeration of the particles takes place by selective adsorption of SDS on NiO particle surfaces. The recovery of electrolyte particles thus increases to 60% with 2×10^{-3} M of SDS. Simultaneously, the transfer of NiO particles to the aqueous phase occurs and this can be explained by the direction of the surfactant heading outwards when the alkyl tails hydrophobically interact with the NiO surface. However, it is not clear how the surfactant and NiO physicochemically interact, and further investigation is needed.

When sonication is included as part of the experiment in the mixing step, the large clusters in the suspensions break down into smaller agglomerates or even primary particles, and they cause better stabilization of hydrophilic particles in the AP. Common ultrasonic processes have been utilized for effective stabilization of nanoparticles.[59] The first hypothesis for this behavior is that ultrasonic treatment is well known to reduce the hydrophobicity of a solid surface, not only protein but also alumina.[63,64] To determine whether ultrasound affects the hydrophobicity of NiO, the samples were sonicated in an ultrasonic bath, when the wettability of individual NiO phases as a function of pH was tested (*cf.* Fig. 5). However, there was no observed particle transfer. This implies that the effect of ultrasound on the particle surface is negligible in this setup which also supports the idea that the effect of sonication on the suspension is a physical change and not a result of sonochemical reactions. The physical effects of ultrasound are typically most robust near system boundaries and interfaces.[65] The lower frequencies of ultrasound responsible for cavitation might cause entrapped

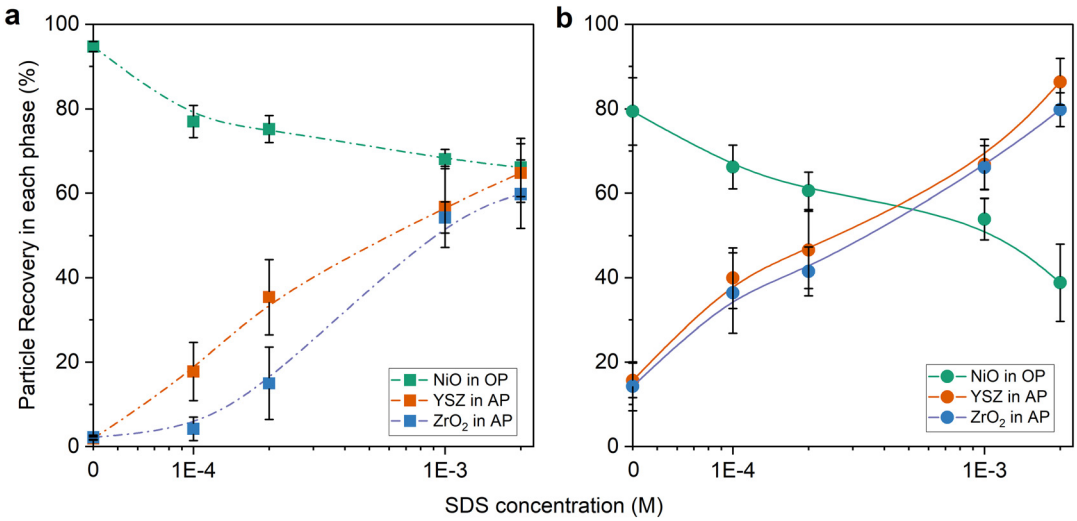

Fig. 7 Mass percentage of the recovered particles in the target phases (NiO in the organic phase (OP) and YSZ and ZrO_2 in the aqueous phase (AP)) by means of LLPS. (a) Without sonication treatment; (b) including a sonication process during experiments. The lines are guides for the eye and the error bars indicate 95% of confidence interval.

electrolyte particles to be released, hence higher AP recoveries as seen in Fig. 7. A combination of surfactants and ultrasonic treatment increases the recovery rate to 80–90% of solid electrolyte particles in the target AP. As stated before, the surfactants decrease the interfacial tension between oil and water. Thus, the transfer of large amounts of particles is possible. However, the high concentration of SDS results in the transfer of more NiO particles to the undesired aqueous phase. Many studies have already demonstrated that sonication and surfactants influence the physicochemical properties of particles but most of these studies aim to improve the dispersion.[31,64]

According to a study from de Aguiar *et al.*, hydrophobic chains of the surfactant were not oriented to the oil phase in parallel but along the interface surface, which is different from the alignment at the water–vapor interface.[66,67] They have found the gauche defects of the SDS alkyl chain while the surfactant comes into contact with the oil phase by analyzing the molecular structures of SDS and the oil phases. These defects cause the conformational disorder of the tail chain and the larger surfactant surface area (*i.e.* hundreds of squared angstroms while the head-group area per SDS is 60 $Å^2$).[68] A size reduction of oil droplets by acoustic cavitation leads to an increase in the contact area between SDS and cyclohexane.[69] The results of their studies indicate that micro-droplets may contribute to an increase in the number of defects in SDS chains. This could potentially explain the observed increase in particles transferring to the AP compared to previous experiments. The defect of the SDS chain observed in their study, however, occurred at the interface between water and oil, suggesting that further research is necessary to gain a deeper understanding of the molecular structure of surfactants at the interface between particles, oil, and water.

3 Conclusions and outlook

The functional layer of HTELs relies on the use of critical raw materials with analogous physical surface properties, which are defined by their wettability. This presents a challenge for the development of a mechanical separation process for recycling. Pivoting on the particle surface charge, different types of surfactants are studied: cationic CTAB for negatively charged solid electrolyte particles and anionic SDS for positively charged electrode particles. This study investigates the influence of surfactants on particle–liquid interfacial behaviour for ultrafine particle selective separation. This method has demonstrated significant potential in the context of recycling HTEL cells. The presence of surfactants decreases the interfacial tension between two immiscible liquids and changes the wettability of the particulates from hydrophilic to hydrophobic. Meanwhile, the air side active material (*i.e.* LSM) exhibited magnetic characteristics, suggesting that high gradient magnetic separation could be a potential future separation process for this fraction. In individual LLPS investigations the surfactant-based separation potential was demonstrated, and a particle mixture separation procedure was concluded.

In consideration of both the distinct NiO behavior with hydrophobic pH-dependent surface properties and the physical effects of sonication, particle mixtures (NiO, YSZ and ZrO_2) have been separated by LLPS. We investigated the impact of pH, with focus on the surfactant concentration as a primary influencing parameter of surfactant adsorption. Temperature is not considered a significant influencing parameter. The surfactant and ultrasonic treatment facilitate the breakdown of hetero-coagulated particles and direct them towards the desired phases. Remarkably, the recovery of hydrophilic particles increases to over 80% in the target phase. However, the simultaneous application of these two parameters has an unfavourable impact on the recovery of NiO within the organic phase. Consequently, a more detailed examination of the adsorption process of the Ni phase with surfactants is required, in addition to fundamental studies on the natural hydrophobicity of NiO. Furthermore, the specific mechanism underlying hetero-coagulation in a range of particle dispersions is required to be identified. Conducting LLPS with only two types of particles could provide better understanding of the particle interactions and their stability. The further consideration of adding different types of salts has the potential to enhance the effectiveness of particle separation processes by the interactions between surfactants and ions.[70] In addition, future studies should investigate the potential benefits of applying ultrasonic treatment prior to the addition of organic solvents or by increasing the number of separation stages with appropriate surfactant washing (multi-stage liquid–liquid separation) in order to enhance the efficiency of the separation process and facilitate process scale-up.[36] Our method can be scaled up for industrial applications, providing a feasible solution for large-scale recycling operations. The process may also lead to a potential reduction in the overall cost of the water electrolysis system. This could make the technology more economically viable and competitive in the energy market. The removal or degradation of the remaining surfactant must be taken into account for industrial applications in order to minimize the environmental impact of contamination and for considerations of water recirculation.[71]

4 Experimental section

4.1 Materials

Pristine single particle fractions used to make HTEL membranes are used in this study. As electrode materials, nickel oxide (Ni(II)O, Product No. GF63811795) and lanthanum strontium manganite (LSM, $La_{0.8}Sr_{0.2}MnO_3$, Product No. 704296) are selected and for the solid electrolyte powder, zirconium(IV) oxide (ZrO_2, Product No. 544760) and yttrium-stabilized zirconia (YSZ, Product No. 464228) are chosen. All the fine particles are purchased from Sigma Aldrich, Germany, and used as received. In addition, two types of surfactants are considered for further investigations.

A cationic surfactant, cetrimonium bromide (CTAB, $[(C_{16}H_{33})N(CH_3)_3]Br$, Product No. 9161) and an anionic surfactant, sodium dodecyl sulfate (SDS, $CH_3(CH_2)_{11}OSO_3Na$, Product No. 0183) are purchased from Carl Roth GmbH, Germany. Cyclohexane (C_6H_{12}, 99.5%, Product No. 6570) from Carl Roth is used as an organic liquid for the particle separation experiments. All materials were used as received.

4.2 Characterization of particle physical properties

Understanding the surface properties of ultrafine particulates in HTELs plays an essential role in developing mechanical separation processes, therefore physical properties such as the particle size distribution, static water contact angle, particle charge, and specific surface area are determined. All measurements are repeated at least three times.

Particle size distributions are determined by using a HELOS laser diffractometer from Sympatec, Germany, with a RODOS dry dispersing unit at 3 bar. The estimated average particle sizes ($d_{50.3}$) are approximately 1 μm for NiO, LSM and YSZ, while that of ZrO_2 is 2.2 μm. Additionally, 90% of all types of particles have a size smaller than 10 μm confirming that all fractions are ultrafine (*cf.* Fig. S1 in the ESI†). More detailed information can be found in Table 2.

For determining the wettability of the particles, a water contact angle is measured by means of a static sessile drop on a particle bed adhered to adhesive carbon patches. After the attachment of dry powders on the surface of the patches, a water droplet is gently placed on three different positions of the substrate and the contact angles are measured using an optical contour analysis device (OCA 50 Pro) from Dataphysics, Germany. All model particles used in this study are known to be intrinsically hydrophilic, attributed to the presence of superficial oxygen layers and metal cations on the surface resulting in a relatively high surface energy. The average values of the water contact angles are summarized below. As expected, the measured apparent contact angle of all particles is below 40°s, as shown in Table 2 and the images of a captive bubble can be found in Fig. S2 in the ESI.†

The specific surface area of each particle fraction is determined by the Brunauer–Emmett–Teller (BET) method using a Gemini VII from Micromeritics Instrument Corp. Prior to measurements, all samples were degassed at 200 °C for 4 hours and the analysis was carried out with N_2 gas. As shown in the table, the surface areas are in order from largest to smallest: NiO, ZrO_2, YSZ and LSM.

In order to characterize the particle surface charge, the double layer potential at a shear plane through electrokinetic phenomena, *i.e.* the zeta potential, is determined by measuring the electroacoustic response and by ultrasonic attenuation measurements with an AcoustoSizer II from Colloidal Dynamics, USA. 10 mM KCl is used as an indifferent electrolyte in all experiments. The range of pH values is between 4 and 11 and adjusted with 1 M hydrochloric acid and 1 M sodium hydroxide. The solid electrolyte materials, YSZ and ZrO_2 show an iso-electric point (IEP) at around pH 8, which is consistent with a previous study on zirconia powders.[72] The electrode materials, NiO and LSM have positively charged surfaces throughout the observed pH range not resulting in an IEP. The effect of pH on zeta potentials of the used materials can be found in Fig. S3 in the ESI.† By comparing the IEP of electrode particles with other studies, the value is different from each other, and it is derived from the sample preparation processes.[72]

On account of the similar physical properties of the used materials, surface charge plays an important role in the separation processes. The four materials can be categorized into two groups with regard to the surface charge between pH 9 and pH 11. In this range, cationic surfactants may be attached to the negatively charged particle surface and render it hydrophobic, while positively charged particles may be altered in their wettability by adding anionic surfactants.

4.3 Methods determining separability

Prior to designing a mechanical separation process, the investigation of surfactant characteristics is carried out. The influence of surfactants on the interface between two immiscible liquids is identified by measuring the interfacial tension. Surface property changes of the respective particles in accordance with different surfactants are evaluated by assessing the zeta potential changes upon adsorption, by measuring the attachment of the particles to a single droplet as a method to quantify their hydrophobicity, and by the LLPS method.

The inverted pendant drop method is used with the OCA 50 Pro system to determine the interfacial tension between cyclohexane and water. The aqueous phase is filled in a cuvette, and the inverted tip is immersed in the solution. A constant volume of a cyclohexane droplet (30 μl) is generated at the end of the needle and its shape is optically analyzed with the Young–Laplace-equation. Interfacial tensions with recorded droplet profiles are measured continuously for 20 min at 20 °C. The measurements are conducted in triplicates after they reach equilibrium and are averaged.

To indirectly assess the adsorption of surfactants on the particle surface, zeta potentials of the particle are determined in the presence of the corresponding surfactant at pH 10. For the positively charged electrode materials, NiO and LSM, the adsorption of the anionic surfactant is anticipated. In contrast, catalyst materials, YSZ and ZrO_2 are negatively charged so that the cationic surfactant, CTAB, may interact and be adsorbed on the particle surface. The measurement procedure is equivalent to the method described in the characterization section. When on average the particle surface is fully covered by the surfactant, an iso-electric point is observed due to the charge compensation. By adding an excess amount of surfactant, a bilayer or so called admicelle may be formed, and the zeta potential will change depending on the charged head group.

Particle attachment to a single droplet is observed with the OCA 50 Pro and after a given time of collision the surface coverage of the droplet with particles is determined as described by Yang *et al.*[73] Based on this method, change in wettability of the particle surface after the conditioning can be evaluated visually as well as quantitatively. A single cyclohexane droplet is generated at the end of a silanized syringe. The images of droplets are taken with a high resolution camera (OCA 50, Dataphysics Instruments) after the mixing step for collision and attachment is stopped and the particles are allowed to settle.

Within two immiscible liquids (water and an insoluble organic solvent) it is possible to separate particles by means of phase transfer, which is dependent on their surface properties. Upon adsorption of surfactant molecules on the particle surface, they may transfer to the organic phase. For the experiment, individual particle fractions are prepared at pH 10 in DI water and conditioned in the presence of each type of surfactant. After conditioning, an equivalent amount of cyclohexane is added and the suspension is manually agitated. The surfactant adsorbed particles can penetrate the interface and be transferred to the organic phase.

In compliance with the results of investigations as mentioned earlier, selective separation of a model particle mixture is carried out with LLPS. The principle of the method is the same as phase separation. After the preliminary tests with various reagents under different pH conditions, the most reasonable combination is determined (*cf.* Fig. 6). The quantification of the recovered particle mixture from each liquid phase is analyzed by X-ray fluorescence (XRF). The data from XRF are validated with standard samples before the experiments, showing a good linear correlation between the known value and the measured value. (R^2 (Ni) = 0.98 and R^2 (Y) = 0.97, R^2 (Zr) = 0.95). Elemental analysis in mass fraction of the recovered particles in each phase is obtained by XRF. These values are converted using the determined calibration curves. The weight percentage of each material is calculated based on their stoichiometry and converted to the normalized value. The recovery rate is calculated based on the ratio of the final concentration and the initial concentration of each element.

Data availability

The authors confirm that the data supporting the findings of this study are available within the article and its ESI.† Raw data that support the findings of this study are available from the corresponding author, upon reasonable request.

Author contributions

Sohyun Ahn: data curation, investigation, methodology, validation, visualization, writing – original draft, writing – review & editing. Suvarna Patil: writing – review & editing. Martin Rudolph: conceptualization, supervision, writing – review & editing.

Conflicts of interest

There are no conflicts to declare.

Acknowledgements

The authors would like to thank the German Federal Ministry for Education and Research (BMBF) for funding of the project ReNaRe – Recycling – Nachhaltige Ressourcennutzung (Grant No.: 03HY111D, FeinElSep) as part of the technology platform H2Giga. The authors acknowledge the help of Rocco Naumann and Klaus Graebe from the Helmholtz Institute Freiberg for Resource Technology for their assistance in the lab.

References

1 E. Commission, *A hydrogen strategy for a climate-neutral EUROPEAN COMMISSION*, 2020, **https://energy.ec.europa.eu/system/files/2020-07/hydrogen_strategy_0.pdf**.
2 F. Dawood, M. Anda and G. M. Shafiullah, Hydrogen production for energy: An overview, *Int. J. Hydrogen Energy*, 2020, **45**, 3847–3869.
3 G. Kakoulaki, I. Kougias, N. Taylor, F. Dolci, J. Moya and A. Jäger-Waldau, Green hydrogen in Europe–A regional assessment: Substituting existing production with electrolysis powered by renewables, *Energy Convers. Manage.*, 2021, **228**, 113649.
4 V. Madadi Avargani, S. Zendehboudi, N. M. Cata Saady and M. B. Dusseault, A comprehensive review on hydrogen production and utilization in North America: Prospects and challenges, *Energy Convers. Manage.*, 2022, **269**, 115927.
5 S. Shiva Kumar and H. Lim, An overview of water electrolysis technologies for green hydrogen production, *Energy Rep.*, 2022, **8**, 13793–13813.
6 M. El-Shafie, Hydrogen production by water electrolysis technologies: A review, *Results Eng.*, 2023, **20**, 101426.
7 M. Nasser, T. F. Megahed, S. Ookawara and H. Hassan, A review of water electrolysis–based systems for hydrogen production using hybrid/solar/wind energy systems, *Environ. Sci. Pollut. Res.*, 2022, **29**, 86994–87018.
8 A. Brisse, J. Schefold and M. Zahid, High temperature water electrolysis in solid oxide cells, *Int. J. Hydrogen Energy*, 2008, **33**, 5375–5382.
9 A. Carbone, S. C. Zignani, I. Gatto, S. Trocino and A. S. Aricò, Assessment of the FAA3-50 polymer electrolyte in combination with a $NiMn_2O_4$ anode catalyst for anion exchange membrane water electrolysis, *Int. J. Hydrogen Energy*, 2020, **45**, 9285–9292.
10 Q. Fang, L. Blum, N. H. Menzler and D. Stolten, *ECS Trans.*, 2017, 2885–2893.
11 O. Schmidt, A. Gambhir, I. Staffell, A. Hawkes, J. Nelson and S. Few, Future cost and performance of water electrolysis: An expert elicitation study, *Int. J. Hydrogen Energy*, 2017, **42**, 30470–30492.
12 C. Mendonça, A. Ferreira and D. M. F. Santos, Towards the commercialization of solid oxide fuel cells: Recent advances

in materials and integration strategies, *Fuels*, 2021, **2**, 393–419.
13 S. Harboe, A. Schreiber, N. Margaritis, L. Blum, O. Guillon and N. H. Menzler, Manufacturing cost model for planar 5 kWel SOFC stacks at Forschungszentrum Jülich, *Int. J. Hydrogen Energy*, 2020, **45**, 8015–8030.
14 M. A. Laguna-Bercero, Recent advances in high temperature electrolysis using solid oxide fuel cells: A review, *J. Power Sources*, 2012, **203**, 4–16.
15 A. Nechache and S. Hody, Alternative and innovative solid oxide electrolysis cell materials: A short review, *Renewable Sustainable Energy Rev.*, 2021, **149**, 111322.
16 Z. Ouyang, Y. Komatsu, A. Sciazko, N. Katsuhiko and N. Shikazono, In-operando observations of Ni-YSZ patterned fuel electrodes under SOFC and SOEC operations, *ECS Trans.*, 2021, **103**, 1219.
17 A. M. Férriz, A. Bernad, M. Mori and S. Fiorot, End-of-life of fuel cell and hydrogen products: A state of the art, *Int. J. Hydrogen Energy*, 2019, **44**, 12872–12879.
18 European Commission, Smes, M. Grohol and C. Veeh, *Study on the critical raw materials for the EU 2023: Final report*, publications office of the European Union, 2023.
19 S. Sarner, A. Schreiber, N. H. Menzler and O. Guillon, Recycling strategies for solid oxide cells, *Adv. Energy Mater.*, 2022, **12**, 2201805.
20 A. Rout, S. Wellens and K. Binnemans, Separation of rare earths and nickel by solvent extraction with two mutually immiscible ionic liquids, *RSC Adv.*, 2014, **4**, 5753–5758.
21 J. Lastam, D. Sergeev, D. Grüner, M. Müller and R. Schwaiger, Unlocking the value of end-of-life JÜLICH solid oxide cell stack interconnect assembly: A combined experimental and thermodynamic study on metallic resource recyclability, *Metals*, 2024, **14**, 406.
22 L.-F. Zhou, D. Yang, T. Du, H. Gong and W.-B. Luo, The current process for the recycling of spent lithium ion batteries, *Front. Chem.*, 2020, **8**, 578044.
23 A. Vanderbruggen, A. Salces, A. Ferreira, M. Rudolph and R. Serna-Guerrero, Improving separation efficiency in end-of-life lithium-ion batteries flotation using attrition pre-treatment, *Minerals*, 2022, **12**, 72.
24 A. Al Assadi, D. Goes, S. Baazouzi, M. Staudacher, P. Malczyk, W. Kraus, F. Nägele, M. F. Huber, J. Fleischer, U. Peuker and K. P. Birke, Challenges and prospects of automated disassembly of fuel cells for a circular economy, *Resour. Conserv. Recycl. Adv.*, 2023, **19**, 200172.
25 C. Kaiser, T. Buchwald and U. A. Peuker, Ultrasonic decoating as a new recycling path to separate oxygen side layers of solid oxide cells, *Green Chem.*, 2024, **26**, 960–967.
26 S. M. Bulatovic, *Handbook of flotation reagents: Chemistry*, Elsevier Science, 2014.
27 K. Holmberg, *Handbook of applied surface and colloid chemistry*, Wiley, 2002.
28 A. Bhattarai, T. Niraula and S. Chatterjee, Sodium dodecyl sulphate: A very useful surfactant for scientific invetigations, *J. Knowl. Innov.*, 2014, **2**, 111–113.
29 A. P. G. Lockwood, P. K. Shun, J. Peakall, N. J. Warren, T. Barber, N. Basharat, G. Randall, M. Barnes, D. Harbottle and T. N. Hunter, Flotation using sodium dodecyl sulphate and sodium lauroyl isethionate for rapid dewatering of $Mg(OH)_2$ radwaste suspensions, *RSC Adv.*, 2021, **11**, 18661–18675.
30 A. Barhoum, H. Rahier, R. E. Abou-Zaied, M. Rehan, T. Dufour, G. Hill and A. Dufresne, Effect of cationic and anionic surfactants on the application of calcium carbonate nanoparticles in paper coating, *ACS Appl. Mater. Interfaces*, 2014, **6**, 2734–2744.
31 A. Asadi, M. Asadi, M. Siahmargoi, T. Asadi and M. Gholami Andarati, The effect of surfactant and sonication time on the stability and thermal conductivity of water-based nanofluid containing $Mg(OH)_2$ nanoparticles: An experimental investigation, *Int. J. Heat Mass Transfer*, 2017, **108**, 191–198.
32 A. B. D. Haan, H. B. Eral and B. Schuur, Industrial Separation Processes Chapter 5, Liquid–Liquid Extraction, in *Fundamentals*, De Gruyter, 2020, pp. 117–154.
33 E. Pramauro and E. Pelezetti, Chapter 7 Surfactant-based extraction and concentration methods, in *Comprehensive Analytical Chemistry*, Elsevier, 1996, vol. 31, pp. 393–451.
34 B. Hu, Y. Nakahiro and T. Wakamatsu, The effect of organic solvents on the recovery of fine mineral particles by liquid-liquid extraction, *Miner. Eng.*, 1993, **6**, 731–742.
35 S. Machunsky and U. A. Peuker, Liquid-liquid interfacial transport of nanoparticles, *Phys. Sep. Sci. Eng.*, 2007, **2007**, 034832.
36 A. Otsuki, G. Mei, Y. Jiang, M. Matsuda, A. Shibayama, J. Sadaki and T. Fujita, Solid-solid separation of fluorescent powders by liquid-liquid extraction using aqueous and organic phases, *Resour. Proc.*, 2006, **53**, 121–133.
37 H. Shergold and O. Mellgren, Concentration of minerals at the oil/water interface, *Trans. Soc. Min. Eng. AIME*, 1970, **247**, 149–159.
38 R. M. E. Silva, R. Poon, J. Milne, A. Syed and I. Zhitomirsky, New developments in liquid-liquid extraction, surface modification and agglomerate-free processing of inorganic particles, *Adv. Colloid Interface Sci.*, 2018, **261**, 15–27.
39 S. Ahn and M. Rudolph, Development of fine particle mechanical separation processes with representative catalyst materials for recycling PEM water electrolyzers exploiting their wetting characteristics, *ChemCatChem*, 2024, **16**, e202300931.
40 H.-J. Butt, K. Graf and M. Kappl, *Physics and Chemistry of Interfaces*, Wiley-VCH, 2003.
41 A. A. Novikov, A. P. Semenov, V. Monje-Galvan, V. N. Kuryakov, J. B. Klauda and M. A. Anisimov, Dual action of hydrotropes at the water/oil interface, *J. Phys. Chem. C*, 2017, **121**, 16423–16431.
42 M. J. Rosen and J. T. Kunjappu, *Surfactants and Interfacial Phenomena*, John Wiley & Sons, 2012.
43 C. Zener, Interaction between the d-shells in the transition metals. II. Ferromagnetic compounds of manganese with perovskite structure, *Phys. Rev.*, 1951, **82**, 403–405.
44 A. O. Turky, M. M. Rashad, A. M. Hassan, E. M. Elnaggar and M. Bechelany, Optical, electrical and magnetic

properties of lanthanum strontium manganite $La_{1-x}Sr_xMnO_3$ synthesized through the citrate combustion method, *Phys. Chem. Chem. Phys.*, 2017, **19**, 6878–6886.

45 R. Mahendiran, S. K. Tiwary, A. K. Raychaudhuri, T. V. Ramakrishnan, R. Mahesh, N. Rangavittal and C. N. R. Rao, Structure, electron-transport properties, and giant magnetoresistance of hole-doped $LaMnO_3$ systems, *Phys. Rev. B: Condens. Matter Mater. Phys.*, 1996, **53**, 3348–3358.

46 Z. L. Peter Boelens, B. Drobot, M. Rudolph, Z. Li, M. Franzreb and K. E. A. F. Lederer, High- gradient magnetic separation of compact fluorescent lamp phosphors: Elucidation of the removal dynamics in a rotary permanent magnet separator, *Minerals*, 2021, **11**, 1116.

47 J. W. Goodwin, Chapter 4. Forces of Repulsion, in *Colloids and Interfaces with Surfactants and Polymers*, Wiley, 2004, pp. 95–125.

48 A. P. Christian, Applications of Surfactants and Nanoparticles in Enhanced Oil Recovery Processes, in *Sedimentary Petrology*, ed. A.-J. Ali Ismail, IntechOpen, 2022, ch. 3.

49 H. H. Kung, *Transition Metal Oxides: Surface Chemistry And Catalysis*, Elsevier, 1989.

50 P. R. Norton, R. L. Tapping and J. W. Goodale, A photoemission study of the interaction of Ni(100), (110) and (111) surfaces with oxygen, *Surf. Sci.*, 1977, **65**, 13–36.

51 N. Hernández, R. Moreno, A. Sánchez-Herencia and J. Fierro, Surface behavior of nickel powders in aqueous suspensions, *J. Phys. Chem. B*, 2005, **109**, 4470–4474.

52 H. Su, Y. Ye, K.-J. Lee, J. Zeng and E. J. Crumlin, Probing the nickel corrosion phenomena in alkaline electrolyte using tender X-ray ambient pressure X-ray photoelectron spectroscopy, *J. Phys. D: Appl. Phys.*, 2021, **54**, 374001.

53 F. J. Micale, M. Topić, C. L. Cronan, H. Leidheiser and A. C. Zettlemoyer, Surface properties of $Ni(OH)_2$ and NiO. I. Water adsorption and heat of immersion of $Ni(OH)_2$, *J. Colloid Interface Sci.*, 1976, **55**, 540–545.

54 Y.-H. Chang, N. Y. Hau, C. Liu, Y.-T. Huang, C.-C. Li, K. Shih and S.-P. Feng, A short-range ordered–disordered transition of a $NiOOH/Ni(OH)_2$ pair induces switchable wettability, *Nanoscale*, 2014, **6**, 15309–15315.

55 G. Azimi, R. Dhiman, H.-M. Kwon, A. T. Paxson and K. K. Varanasi, Hydrophobicity of rare-earth oxide ceramics, *Nat. Mater.*, 2013, **12**, 315–320.

56 M. J. Eslamibidgoli, A. Groß and M. Eikerling, Surface configuration and wettability of nickel(oxy)hydroxides: A first-principles investigation, *Phys. Chem. Chem. Phys.*, 2017, **19**, 22659–22669.

57 B. Kronberg, Surfactant mixtures, *Curr. Opin. Colloid Interface Sci.*, 1997, **2**, 456–463.

58 Y. R. Wang and W. Chu, Degradation of a xanthene dye by Fe(II)-mediated activation of oxone process, *J. Hazard. Mater.*, 2011, **186**, 1455–1461.

59 A. Asadi, F. Pourfattah, I. Miklós Szilágyi, M. Afrand, G. Żyła, H. Seon Ahn, S. Wongwises, H. Minh Nguyen, A. Arabkoohsar and O. Mahian, Effect of sonication characteristics on stability, thermophysical properties, and heat transfer of nanofluids: A comprehensive review, *Ultrason. Sonochem.*, 2019, **58**, 104701.

60 A. M. Islam, B. Z. Chowdhry and M. J. Snowden, Heteroaggregation in colloidal dispersions, *Adv. Colloid Interface Sci.*, 1995, **62**, 109–136.

61 N. Mishchuk, Electric double layer and electrostatic interaction of hydrophobic particles, *J. Colloid Interface Sci.*, 2008, **320**, 599–607.

62 P. Hu and L. Liang, The role of hydrophobic interaction in the heterocoagulation between coal and quartz particles, *Miner. Eng.*, 2020, **154**, 106421.

63 V. Belova, D. A. Gorin, D. G. Shchukin and H. Möhwald, Controlled effect of ultrasonic cavitation on hydrophobic/hydrophilic surfaces, *ACS Appl. Mater. Interfaces*, 2011, **3**, 417–425.

64 M. Anwar Ul Alam, A. Kassu and L. S. Kassama, Effect of sonication time and surfactant concentration on improving the bio-accessibility of lycopene synthesized in poly-lactic co-glycolic acid nanoparticles, *arXiv*, 2023, preprint, arXiv:2301.10850, DOI: **10.13031/aim.202200474**.

65 S. Kentish and M. Ashokkumar, The Physical and Chemical Effects of Ultrasound, in *Ultrasound Technologies for Food and Bioprocessing*, ed. H. Feng, G. Barbosa-Canovas and J. Weiss, Springer, New York, 2011, pp. 1–12.

66 H. B. de Aguiar, M. L. Strader, A. G. F. de Beer and S. Roke, Surface structure of sodium dodecyl sulfate surfactant and oil at the oil-in-water droplet liquid/liquid interface: A manifestation of a nonequilibrium surface state, *J. Phys. Chem. B*, 2011, **115**, 2970–2978.

67 R. Vácha and S. Roke, Sodium dodecyl sulfate at water–hydrophobic interfaces: A simulation study, *J. Phys. Chem. B*, 2012, **116**, 11936–11942.

68 M. Almgren and S. Swarup, Size of sodium dodecyl sulfate micelles in the presence of additives. 3. Multivalent and hydrophobic counterions, cationic and nonionic surfactants, *J. Phys. Chem.*, 1983, **87**, 876–881.

69 T. S. H. Leong, T. J. Wooster, S. E. Kentish and M. Ashokkumar, Minimising oil droplet size using ultrasonic emulsification, *Ultrason. Sonochem.*, 2009, **16**, 721–727.

70 H. Garmsiri, S. Jahani, Y. Kazemzadeh, M. Sharifi, M. Riazi and R. Azin, Stability of the emulsion during the injection of anionic and cationic surfactants in the presence of various salts, *Sci. Rep.*, 2023, **13**, 11337.

71 J. Arora, A. Ranjan, A. Chauhan, R. Biswas, V. D. Rajput, S. Sushkova, S. Mandzhieva, T. Minkina and T. Jindal, Surfactant pollution, an emerging threat to ecosystem: Approaches for effective bacterial degradation, *J. Appl. Microbiol.*, 2022, **133**, 1229–1244.

72 W.-C. J. Wei, S.-C. Wang and F.-Y. Ho, Electrokinetic properties of colloidal zirconia powders in aqueous suspension, *J. Am. Ceram. Soc.*, 1999, **82**, 3385–3392.

73 H. Yang, Y. Xing, L. Sun, Y. Cao and X. Gui, Kinetics of bubble-particle attachment and detachment at a single-bubble scale, *Powder Technol.*, 2020, **370**, 251–258.